

Nonclassical Chiral Elasticity of the Gyroid Lattice

D. R. Reasa and R. S. Lakes^{*}*Department of Engineering Physics, University of Wisconsin, Madison, Wisconsin 53706, USA* (Received 11 June 2020; accepted 17 September 2020; published 13 November 2020)

The gyroid lattice is a metamaterial which allows chirality that is tunable by geometry. Gyroid lattices were made in chiral and nonchiral form by 3D printing. The chiral lattices exhibited nonclassical elastic effects including coupling between compressive stress and torsional deformation. Gyroid lattices can approach upper bounds on elastic modulus. Effective modulus is increased by distributed moments but is, for gyroid cylinders of sufficiently small radius, softened by a surface layer of incomplete cells. Such size dependence is similar to that in foams but is unlike most lattices.

DOI: [10.1103/PhysRevLett.125.205502](https://doi.org/10.1103/PhysRevLett.125.205502)

Spatially periodic surface lattices including gyroid lattices were originally introduced [1–3] for their potential as lightweight stiff and strong structures. Periodic surfaces including the gyroid are of interest in crystallography [4]. Periodic shell lattices have been analyzed in the context of multifunctional capability such as for simultaneous transport of heat and electricity [5]. Gyroid surfaces [6] were studied in relation to the Landau-Ginzburg Hamiltonian for microemulsions [7] in which energy is minimized during phase segregation. Gyroid structures can be formed by self-assembly [8]; they occur in butterfly wings and give rise to interesting optical properties [9] and are known as photonic crystals. It was suggested that butterflies grow these gyroid structures on the nanoscale via self-organizing processes in lipid bilayer membranes. Optical properties of gyroids have been studied in the context of enhanced electrochromism in vanadium pentoxide [10]. Gyroids of space group $Ia\bar{3}d$ [11] appear via energy minimization in block copolymers [12,13]. The gyroid is of particular interest because it allows *chirality*.

Physical manifestations of chirality have long been known in chemistry and in physical properties such as piezoelectricity, pyroelectricity, and optical activity [14]. Chirality has no effect in classical elasticity because the elasticity tensor is fourth rank. Elastic chirality is predicted to cause qualitatively new effects in the context of generalized elasticity [15]. Chiral elastic solids can exhibit stretch-twist coupling, size effects in torsion and compression, and radial dependence of the Poisson effect. Experimentally, stretch-twist coupling effects were observed in bone [16] and in tendon fascicles (fiber bundles) [17]. Chiral cholesteric elastomers [18] were predicted to twist in response to stretching with a characteristic length predicted to be on the order of 10 nm.

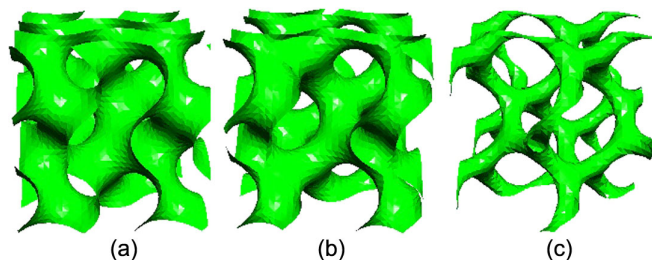
The gyroid surface can be described [11] by

$$\sin 2\pi y \cos 2\pi z + \sin 2\pi z \cos 2\pi x + \sin 2\pi x \cos 2\pi y = t, \quad (1)$$

with t as a constant, as shown in Fig. 1 for $t = 0$, $t = 0.6$, and $t = 1.2$.

The gyroid surface allows chirality as a surface or by dividing space into two connected regions, called labyrinths [4], that (for $t = 0$) are enantiomorphic: they are mirror images of each other. The surface in Eq. (1) is invariant to an inversion operator (the negative of a Kronecker delta), $\hat{a}_{ij} = -\delta_{ij}$ if $t = 0$ and is not invariant otherwise. A choice of nonzero t entails a chiral surface so chirality can be tuned by geometry. One may choose a value of t and embody the gyroid as a shell lattice with nonzero thickness. Alternatively one may fill one of the labyrinths with solid material. In this Letter, nonclassical elastic effects including those of chirality are experimentally demonstrated for the gyroid.

Gyroid lattices were made with a surface wall thickness of 0.4 mm and a cell size of 6 mm. Figure 2 shows the physical lattices. The solid material was a nylon polymer PA 2200 for which the density was $\rho_s = 0.98 \text{ g/cm}^3$, Young's modulus $E_s = 1.6 \text{ GPa}$ and Poisson's ratio 0.4. The ratio of lattice density to the solid density was $\rho/\rho_s = 0.21$ for $t = 0$ and 0.195 for $t = 0.6$ and -0.6 . To make the gyroid lattices, the surface in Eq. (1) was expressed in MATLAB. A 3D point cloud associated with the surface was then obtained and saved as a STL (stereolithography) file. Thickness was added via BLENDER, as were end caps made

FIG. 1. Gyroid lattices. (a) $t = 0$, (b) $t = 0.6$, (c) $t = 1.2$.

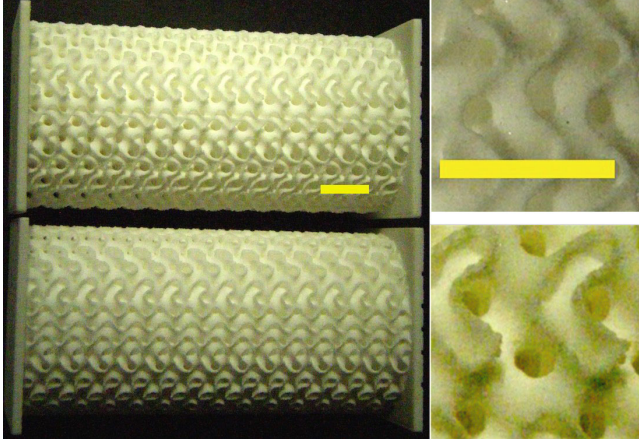


FIG. 2. Polymer gyroid lattices. Bottom: nonchiral, $t = 0$. Top: $t = 0.6$. Right: structure detail. Scale bars 1 cm.

using SOLIDWORKS. The file was postprocessed with NETFABB for export to a EOS P760 3D printer. Aluminum end caps were cemented. Specimens were prepared with length twice the diameter.

As for methods, size dependency of rigidity was measured in torsion and bending via a laser based method [19,20] at 1 Hz. Twist deformation in response to compression under dead weights was determined via a laser beam reflected from a mirror on the specimen to a silicon position sensitive detector. See Supplemental Material for details [21]. Further compression tests revealed the compressive elastic modulus; the Poisson's ratio was determined from analysis of photographs. All tests were done at small strain in the linear domain.

The gyroid lattice is stiffer, per unit density, than foams or rib lattices. The gyroid compressive Young's modulus was $E = 120$ MPa for $t = 0$. For comparison, the gyroid with solid volume fraction $\rho/\rho_s = 0.21$ is a factor 2.1 stiffer than an isotropic truss (rib) lattice, via $E/E_s = \frac{1}{6}[\rho/\rho_s]$. The gyroid modulus approaches the Hashin-Shtrikman upper bound [22,23] if ρ/ρ_s is sufficiently small (for which $E/E_s = \frac{1}{2}[\rho/\rho_s]$) or the solid Poisson's ratio approaches its lower bound; see Supplemental Material for further details [21]. For a volume fraction 0.2, the upper bound is about 10% greater than for low volume fraction, corresponding to $E = 176$ MPa. So the present gyroid lattice exceeds the properties of foams and truss lattices of the same solid phase and has 68% of the upper bound E .

This gyroid lattice is nearly isotropic in its classical elastic properties though it has cubic symmetry. The degree of anisotropy is revealed by the Zener ratio $Z = 2G(1 + \nu)/E$ with G as shear modulus and Poisson's ratio $\nu = 0.27$ in the absence of gradients. For the gyroid with $t = 0$, $Z = 0.99$; for perfect isotropy, $Z = 1$. Elastic isotropy is advantageous for many applications.

Chirality is incorporated in elasticity via the following nonclassical constitutive equations [15] that allow a degree

of nonlocal response. The material is assumed to be isotropic with respect to direction but is not invariant to inversions.

$$\begin{aligned} \sigma_{kl} = & \lambda \epsilon_{rr} \delta_{kl} + 2G \epsilon_{kl} + \kappa e_{klm} (r_m - \phi_m) \\ & + C_1 \phi_{r,r} \delta_{kl} + C_2 \phi_{k,l} + C_3 \phi_{l,k}, \end{aligned} \quad (2)$$

$$\begin{aligned} m_{kl} = & \alpha \phi_{r,r} \delta_{kl} + \beta \phi_{k,l} + \gamma \phi_{l,k} + C_1 \epsilon_{rr} \delta_{kl} \\ & + (C_2 + C_3) \epsilon_{kl} + (C_3 - C_2) e_{klm} (r_m - \phi_m). \end{aligned} \quad (3)$$

The stress σ_{ij} (force per unit area) can be asymmetric. Distributed moments m_{ij} (a torque per unit area) balance the asymmetry. ϵ_{ij} is the strain tensor. The macrorotation is $r_i = (e_{ijk} u_{k,j})/2$ with u as displacement; ϕ_k is the rotation of points or microrotation. Elastic constants λ and G have the same meaning as in classical elasticity. Elastic constants α , β , γ are Cosserat elastic constants which govern the characteristic length scales at which nonclassical effects are to be observed [24,25]. The characteristic length for torsion is $\ell_t = \sqrt{(\beta + \gamma)/2G}$, and for bending, $\ell_b = \sqrt{\gamma/4G}$. Elastic constant κ governs the coupling between local rotation and rotation due to displacement gradient. All six isotropic nonchiral Cosserat elastic constants were obtained experimentally via size effect measurements in torsion and bending [26]. In a noncohesive granular assembly κ was determined via waves [27]; granular flows have been analyzed via Cosserat theory [28].

Elastic constants C_1 , C_2 , and C_3 represent the effect of chirality (noncentrosymmetry). The exact solution for tension or compression of a round chiral Cosserat cylinder [15] enables design and interpretation of experiments on chiral elastic solids. New effects are predicted including stretch-twist coupling, size effects in tension or compression effective modulus, and size effects in Poisson's ratio. The experiments here allow determination of combinations of elastic constants but not all nine.

Nonclassical squeeze-twist coupling b_0/ϵ of the gyroid lattice is shown in Fig. 3; b_0 is the twist angle per length and ϵ is the compressive strain. The nonclassical length parameter A for chirality in Eq. (4) is the product of the torsion characteristic length ℓ_t and a function of various coupling coefficients that depend on the nine elastic constants [15] of a chiral material. B is also a function of the elastic constants. The theory predicts b_0/ϵ to vary in magnitude as $1/r^2$ for sufficiently large specimen radius r :

$$\frac{b_0}{\epsilon} = \frac{A}{\left(\frac{r}{2}\right)^2 + B}. \quad (4)$$

Values of chiral length A for chiral lattices were considerably smaller than the 6 mm cell size and smaller than the characteristic length ℓ_t as shown in Table I. The goodness of fit R was 0.99 or better for nonzero t .

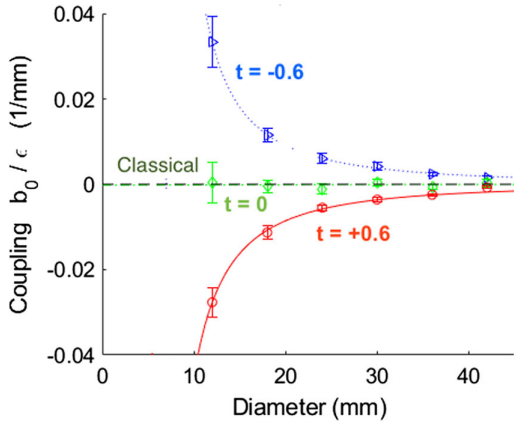


FIG. 3. Nonclassical squeeze-twist coupling in gyroid lattices. Ratio of twist angle per length b_0 to strain ϵ versus specimen diameter $= 2r$ depends on chirality parameter t . Points are experimental; diamonds, $t = 0$; circles, $t = 0.6$; triangles, $t = -0.6$. Curves are fits via Eq. (4). Classical elasticity and nonchiral Cosserat elasticity predict zero squeeze-twist b_0/ϵ , shown by the horizontal dashed line.

The nonchiral gyroid exhibited essentially no squeeze-twist coupling as anticipated. $\sqrt{B} = 0.02$ mm for $t = 0.6$ and 0.11 mm for $t = -0.6$; the fit is insensitive to B because B is too small to noticeably influence the curve shape. The maximum ratio of twist to squeeze was $b_0/\epsilon|_{2\text{cell}} = 0.035/\text{mm}$ for gyroid specimens two cells wide.

For comparison with lattices made of the same base polymer, in a cubic lattice with helical ribs [29] and a cell size of 8.5 mm, the maximum ratio of twist to squeeze was $b_0/\epsilon|_{2\text{cell}} = 0.018/\text{mm}$. Young's modulus was $E = 0.26$ MPa and the shear modulus was $G = 0.0336$ MPa, implying substantial anisotropy. The relative density was $\rho/\rho_s = 0.12$.

Chiral, elastically isotropic rib lattices [30] exhibited a larger maximum squeeze-twist coupling $b_0/\epsilon|_{2\text{cell}} = 0.057/\text{mm}$ for specimens two cells wide. Physical lattices had $E \approx 60$ MPa and relative density $\rho/\rho_s = 0.37$. These lattices had cubical nodules linked by oblique ribs. The chiral gyroid lattices are considerably stiffer than the other chiral lattices, with effective Young's modulus E about 100 MPa.

Elastic chirality of greater magnitude in the gyroid may be sought by varying t . The gyroid remains connected provided $|t| < \sqrt{2}$. Large t presents practical challenges for surfaces of nonzero thickness because as t becomes larger, lattice tubules become thinner, hence more difficult to fabricate.

TABLE I. Gyroid properties.

t	E (MPa)	G (MPa)	ℓ_t (mm)	ℓ_b (mm)	A (mm)
0	120	46.8	1.5	4.7	-0.006
0.6	100	34.6	2.4	2.6	0.28
-0.6	98	33.7	2.9	2.7	-0.24

Nonclassical size effects in torsion of the gyroid lattice are shown in Fig. 4. Size effects are expressed as the rigidity ratio Ω (relative stiffness) versus diameter. Ω is the ratio of observed structural rigidity to the asymptotic rigidity for large diameter.

The four largest specimens exhibited a nonclassical stiffening size effect from which ℓ_t was extracted. The asymptotic shear modulus in the absence of gradients was $G = 34.6$ MPa and the characteristic length for torsion was $\ell_t = 2.4$ mm for $t = 0.6$; $G = 46.8$ MPa and $\ell_t = 1.5$ mm for $t = 0$, and $G = 33.7$ MPa and $\ell_t = 2.9$ mm for $t = -0.6$. Results are consistent with a coupling number $N = \sqrt{\kappa/(2G + \kappa)} = 1$ and a polar ratio $\Psi = (\beta + \gamma)/(\alpha + \beta + \gamma) = 1.5$. The characteristic length ℓ_t is considerably smaller (by a factor 4 for $t = 0$ and by a factor 2 for $t = -0.6$) than the cell size 6 mm. For comparison, open cell foams including negative Poisson's ratio foams exhibited a characteristic length larger than the cell size, a factor 4 for normal foams [20], and large size effects Ω up to a factor of 8. Designed lattices exhibited a characteristic length comparable to the cell size and a large magnitude (a factor 30) of size effect [31]. Particulate composites exhibited no size effects and $\ell_t = 0$ [32]. Chiral isotropic rib lattices [30] exhibited size effects Ω of a factor of more than 4 in torsion with inferred torsion characteristic length 95% of the cell size. The gyroid Ω was much smaller, less than 1.4 for $t = -0.6$ and 1.1 for $t = 0$.

The range of smaller diameter in the gyroid is associated with reduction in torsional stiffness due to incomplete cells at the surface. Such effects are known in foams [33]. Similar effects were observed in bending and compression. Rib lattices with cells that are structurally complete do not exhibit such a stiffness reduction [30,31].

In bending, the larger specimens were about 25% stiffer than anticipated from compression indicating a size effect hence a nonzero bending characteristic length ℓ_b as shown

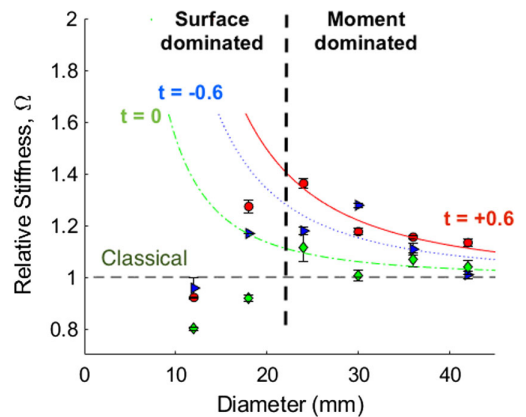


FIG. 4. Nonclassical size effect of gyroid lattices in torsion. Dependence of rigidity ratio Ω on specimen diameter and on t . Points are experimental; diamonds, $t = 0$; circles, $t = 0.6$; triangles, $t = -0.6$. Curves are fits from theory. Classical elasticity predicts $\Omega = 1$, the horizontal dashed line.

in Table I. Bending size effect curves revealed more softening due to incomplete cells than was the case in torsion; therefore, inference of ℓ_b was not as rigorous as for ℓ_t .

Size dependence of the effective elastic modulus E in compression can occur in chiral elastic materials but not in classical elasticity or in nonchiral Cosserat elasticity. The four larger chiral gyroids exhibit a slight stiffening size effect Ω (about a factor 1.2 over the range studied). The corresponding nonchiral specimens varied $\pm 4\%$ in stiffness, attributed to the printing method. For comparison, chiral isotropic rib lattices [30] exhibited a factor of about 2.4 size effect in compression.

The gyroid, as an extremal shell lattice, has superior stiffness and strength compared with truss (rib) lattices. The communicating porosity is considered advantageous in the context of scaffolds for tissue ingrowth [23,34]. Shell and rib lattices can exhibit considerable anisotropy which may not be desirable. The present nonchiral gyroid lattices exhibit a Zener ratio near 1, hence isotropy of the classical elastic behavior. Nonclassical elastic response (squeeze-twist coupling) occurs in chiral gyroid lattices; such effects are anticipated in other gyroids such as those in block copolymers and in biological tissues. Elastic chirality also gives rise to acoustic activity in which the plane of polarization of shear waves rotates. Other even rank tensor properties such as thermal expansion do not reveal chirality, but corresponding general theories that admit distributed moments allow nonclassical effects of chirality. Nonclassical elasticity can offer advantages in reducing concentrations of stress and strain [35] and can occur at the nanoscale [36]. Chiral squeeze-twist coupling may be beneficial in sensors and actuators.

The authors gratefully acknowledge support of this research by the National Science Foundation via Grant No. CMMI-1906890.

*Corresponding author.
lakes@engr.wisc.edu

- [1] A. H. Schoen, Infinite regular warped polyhedra and infinite periodic minimal surfaces, *Am. Math. Soc.* **30**, 23 (1968).
- [2] A. H. Schoen, Infinite periodic minimal surfaces without self-intersections, NASA Report No. TN D-5541, 1970.
- [3] A. H. Schoen, Reflections concerning triply-periodic minimal surfaces, *Interface Focus* **2**, 658 (2012).
- [4] W. Fischer and K. Koch, On 3-periodic minimal surfaces, *Z. Kristallogr.* **179**, 31 (1987).
- [5] S. Torquato, S. Hyun, and A. Donev, Multifunctional Composites: Optimizing Microstructures for Simultaneous Transport of Heat and Electricity, *Phys. Rev. Lett.* **89**, 266601 (2002).
- [6] W. Gózdź and R. Hoyst, High Genus Periodic Gyroid Surfaces of Nonpositive Gaussian Curvature, *Phys. Rev. Lett.* **76**, 2726 (1996).
- [7] V. Luzzati, A. Tardieu, T. Gulek-Krzywicki, E. Rivas, and F. Reiss-Husson, Structure of the cubic phases of lipid-water systems, *Nature (London)* **220**, 485 (1968).
- [8] L. J. Ellison, D. J. Michel, F. Barmes, and D. J. Cleaver, Entropy-Driven Formation of the Gyroid Cubic Phase, *Phys. Rev. Lett.* **97**, 237801 (2006).
- [9] V. Saranathan, C. O. Osuji, S. G. J. Mochrie, H. Noh, S. Narayanan, A. Sandy, E. R. Dufresne, and R. O. Prum, Structure, function, and self-assembly of single network gyroid ($I4_132$) photonic crystals in butterfly wing scales, *Proc. Natl. Acad. Sci. U.S.A.* **107**, 11676 (2010).
- [10] M. R. J. Scherer, L. Li, P. M. S. Cunha, O. A. Scherman, and U. Steiner, Enhanced electrochromism in gyroid-structured vanadium pentoxide, *Adv. Mater.* **24**, 1217 (2012).
- [11] M. Wohlgemuth, N. Yufa, J. Hoffman, and E. L. Thomas, Triply periodic bicontinuous cubic microdomain morphologies by symmetries, *Macromolecules* **34**, 6083 (2001).
- [12] M. F. Schulz, F. S. Bates, K. Almdal, and K. Mortensen, Epitaxial Relationship for Hexagonal-to-Cubic Phase Transition in a Block Copolymer Mixture, *Phys. Rev. Lett.* **73**, 86 (1994).
- [13] M. W. Matsen and M. Schick, Stable and Unstable Phases of a Diblock Copolymer Melt, *Phys. Rev. Lett.* **72**, 2660 (1994).
- [14] J. F. Nye, *Physical Properties of Crystals* (Clarendon, Oxford, 1976).
- [15] R. S. Lakes and R. L. Benedict, Noncentrosymmetry in micropolar elasticity, *Int. J. Eng. Sci.* **20**, 1161 (1982).
- [16] R. S. Lakes, Is bone elastically noncentrosymmetric? in *34th ACEMB Annual Conference on Engineering in Medicine and Biology* (1981).
- [17] K. Buchanan, R. S. Lakes, and R. Vanderby, Chiral behavior in rat tail tendon fascicles, *J. Biomech.* **64**, 206 (2017).
- [18] M. Warner, E. M. Terentjev, R. B. Meyer, and Y. Mao, Untwisting of a Cholesteric Elastomer by a Mechanical Field, *Phys. Rev. Lett.* **85**, 2320 (2009).
- [19] T. Lee, R. S. Lakes, and A. Lal, Resonant ultrasound spectroscopy for measurement of mechanical damping: Comparison with broadband viscoelastic spectroscopy, *Rev. Sci. Instrum.* **71**, 2855 (2000).
- [20] Z. Rueger and R. S. Lakes, Cosserat elasticity of negative Poisson's ratio foam: Experiment, *Smart Mater. Struct.* **25**, 054004 (2016).
- [21] See Supplemental Material at <http://link.aps.org/supplemental/10.1103/PhysRevLett.125.205502> for further detail on the experiments and on the interpretation.
- [22] Z. Hashin and S. Shtrikman, A variational approach to the theory of the elastic behaviour of multiphase materials, *J. Mech. Phys. Solids* **11**, 127 (1963).
- [23] S. C. Kapfer, S. T. Hyde, K. Mecke, C. H. Arns, and G. E. Schröder-Turk, Minimal surface scaffold designs for tissue engineering, *Biomaterials* **32**, 6875 (2011).
- [24] E. Cosserat and F. Cosserat, *Theorie des Corps Deformables* (Hermann et Fils, Paris, 1909).
- [25] A. C. Eringen, Theory of micropolar elasticity, in *Fracture*, edited by H. Liebowitz (Academic Press, New York, 1968), Vol. 1, pp. 621–729.
- [26] Z. Rueger and R. S. Lakes, Experimental study of elastic constants of a dense foam with weak Cosserat coupling, *J. Elast.* **137**, 101 (2019).

- [27] A. Merkel and V. Tournat, Experimental Evidence of Rotational Elastic Waves in Granular Phononic Crystals, *Phys. Rev. Lett.* **107**, 225502 (2011).
- [28] N. Mitarai, H. Hayakawa, and H. Nakanishi, Collisional Granular Flow as a Micropolar Fluid, *Phys. Rev. Lett.* **88**, 174301 (2002).
- [29] D. Reasa and R. S. Lakes, Cosserat effects in achiral and chiral cubic lattices, *J. Appl. Mech.* **86**, 111009 (2019).
- [30] C. S. Ha, M. E. Plesha, and R. S. Lakes, Chiral three-dimensional isotropic lattices with negative Poisson's ratio, *Phys. Status Solidi B* **253**, 1243 (2016).
- [31] Z. Rueger and R. S. Lakes, Strong Cosserat Elasticity in a Transversely Isotropic Polymer Lattice, *Phys. Rev. Lett.* **120**, 065501 (2018).
- [32] R. D. Gauthier and W. E. Jahsman, A quest for micropolar elastic constants, *J. Appl. Mech.* **42**, 369 (1975).
- [33] R. Brezny and D. J. Green, Characterization of edge effects in cellular materials, *J. Mater. Sci.* **25**, 4571 (1990).
- [34] F. P. W. Melchels, K. Bertoldi, R. Gabbriellini, A. H. Velders, J. Feijen, and D. W. Grijpma, Mathematically defined tissue engineering scaffold architectures prepared by stereolithography, *Biomaterials* **31**, 6909 (2010).
- [35] R. D. Mindlin, Effect of couple stresses on stress concentrations, *Exp. Mech.* **3**, 1 (1963).
- [36] R. Maranganti and P. Sharma, Length Scales at which Classical Elasticity Breaks Down for Various Materials, *Phys. Rev. Lett.* **98**, 195504 (2007).